Interaction of Particles and Pathogens with Biological Membranes

Thorsten Auth, Sabyasachi Dasgupta, and Gerhard Gompper

Abstract Biological membranes are both barriers and communication interfaces of cells. Transport across membranes is therefore essential for life. It encompasses both endocytotic and exocytotic processes important for cell function, but also the invasion of cells by parasites and viruses, and targeted drug delivery. Whereas interactions on the molecular scale are important for particles with sizes comparable with the thickness of the membrane, the mechanical properties of the entire membrane determine its interaction with larger particles. We focus here on large particles and parasites and discuss wrapping of single particles by homogeneous and complex membranes. Both solid particles with various shapes as well as soft particles are considered. Membrane-mediated interactions of many particles lead to aggregation and tubulation. Finally, active biological mechanisms are shown to support the invasion of parasites, such as the malaria parasite, and to drive phagocytosis.

Keywords Nanoparticles · Helfrich Hamiltonian · Endocytosis · Pathogens · Malaria · Phagocytosis

1 Introduction

Membranes are ubiquitous in biological cells. While the plasma membrane encloses the entire cell, membranes also compartmentalize cells and thereby define organelles. Transmembrane transport is essential for both the intracellular communication and the communication of cells with their environment [16, 60]. The interaction of particles and pathogens with biological membranes—and therefore

T. Auth (✉) · G. Gompper
Forschungzentrum Jülich, Theoretical Soft Matter and Biophysics, Institute of Complex Systems and Institute for Advanced Simulation, Jülich, Germany
e-mail: t.auth@fz-juelich.de; g.gompper@fz-juelich.de

S. Dasgupta
National University of Singapore, Mechanobiology Institute, Singapore, Singapore

P. Bassereau, P. Sens (eds.), *Physics of Biological Membranes*,
https://doi.org/10.1007/978-3-030-00630-3_17

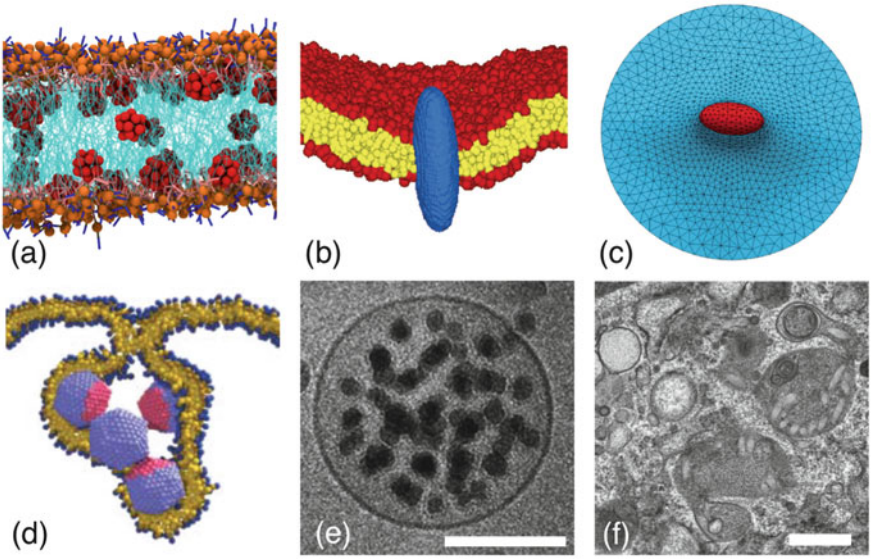

Fig. 1 Interaction of nanoparticles with membranes. (**a**) Incorporation. Fullerenes in a POPC membrane. Reprinted with permission from [10]. Copyright 2014 by the American Physical Society. (**b**) Penetration. An ellipsoidal nanoparticle passes through a lipid bilayer. Adapted by permission from Macmillan Publishers Ltd: Nat. Nanotechnol., [116], Copyright © 2010. (**c**) Wrapping. An ellipsoidal nanoparticle gets wrapped by a lipid bilayer membrane. Reproduced from [31] with permission from The Royal Society of Chemistry. (**d**) Cooperative wrapping. Capsids bud cooperatively. Adapted by permission from Macmillan Publishers Ltd: Nature, [87], Copyright © 2007. (**e**) Cryo-TEM micrographs of nanoparticles incorporated into a vesicle. The length of the scale bar corresponds to 100 nm. Reprinted from [72] with permission from The Royal Society of Chemistry. (**f**) TEM micrographs of nanoparticles internalized in human mesenchymal stem cells. The length of the scale bar corresponds to 500 nm. Adapted with permission from [45]. Copyright © 2012 Wiley-VCH Verlag GmbH & Co. KGaA, Weinheim

also their transport across membranes—crucially depends on the particle size, shape, softness, and surface functionalization. A zoo of engineered nanoparticles can nowadays be fabricated, with sizes from nanometers to micrometers and various shapes, such as spherical, ellipsoidal, cuboidal, dumbbell-shaped, and bullet-shaped [18, 22, 82]. Pathogens are nanometer-sized viruses, such as the filamentous Marburg and Ebola viruses [78, 113], and micrometer-sized parasites, such as the egg-shaped malaria parasite [25, 30]. Figure 1 shows an overview over particle–membrane interactions.

For particles with diameters that are large compared to the thickness of the membrane, the membrane can be modeled using a mathematical surface with curvature-elastic properties. The deformation energy is calculated using the Helfrich Hamiltonian [55], and the attractive interaction between particle and membrane can

be taken into account using a contact energy:

$$\mathscr{H} = \int_S dS \left[\gamma + 2\kappa (H - c_0)^2 + \bar{\kappa} K\right] + w \int_{S_{\mathrm{ad}}} dS\,. \tag{1}$$

The membrane conformation is characterized by the two principal curvatures at each point of the membrane, c_1 and c_2, that enter the Hamiltonian via the mean curvature $H = (c_1 + c_2)/2$ and the Gaussian curvature $K = c_1 c_2$. The total deformation energy is obtained by integration over the entire membrane area S, the adhesion energy by integration over the adhered membrane area S_{ad}. Membrane tension γ, bending rigidity κ, Gaussian saddle-splay modulus $\bar{\kappa}$, and spontaneous curvature c_0 describe the mechanical properties of the membrane; the adhesion strength w characterizes the contact interaction. If we assume a homogeneous membrane and disregard topology changes, i.e., the last step of detachment of a wrapped particle that is still connected via a small neck to the lipid bilayer membrane, the contribution of the Gaussian curvature is constant and given by the Euler characteristic of the surface [1]. Typical values for the bending rigidity are $20\,k_{\mathrm{B}}T < \kappa < 100\,k_{\mathrm{B}}T$, for the membrane tension $10^{-5}\,k_{\mathrm{B}}T/\mathrm{nm}^2 < \gamma < 1\,k_{\mathrm{B}}T/\mathrm{nm}^2$ [103], and for the adhesion strength $2 \times 10^{-6}\,k_{\mathrm{B}}T/\mathrm{nm}^2 < w < 0.2\,k_{\mathrm{B}}T/\mathrm{nm}^2$ [2].

In Sect. 2, wrapping of single spherical and nonspherical particles by homogeneous model membranes is discussed. For tensionless membranes, spherical particles are either not wrapped or completely wrapped by the membrane at low and high adhesion strength, respectively. The transition between these two states is discontinuous. Nonspherical particles show a much more complex wrapping behavior and an increased stability of partial-wrapped states [29]. Soft particles deform while adhering to the membrane, which further increases the stability of partial-wrapped states. We also briefly address dynamical aspects of particle wrapping. For partial wrapping of spherical particles, not only the attached membrane, but also the free membrane around particles and the particle itself gets deformed. Both contribute to the deformation energy.

In Sect. 3, the complexity of the single-particle wrapping scenario is extended to multicomponent biomembranes. Biomembranes can show strong and weak segregation, domain formation and aggregation of lipid and protein components within the membranes, respectively. In Sect. 4, examples for membrane deformation-mediated interaction between particles and for particle self-assembly are presented. In Sect. 5, systems with biological activity are discussed, such as the invasion of the malarial parasite and phagocytosis.

Interaction of Small Particles with Biological Membranes Particles that are comparable with molecular sizes of lipids interact similarly with biological membranes as proteins. Particles with suitable hydrophobicity may penetrate the lipid bilayer [84], which is also observed for cell-penetrating peptides [24] and which has been proposed for amphiphilic polymers [114].

(continued)

Hydrophobic nanoparticles assemble within the tail region of the lipid bilayer [90, 100] and aggregate, probably similar to integral proteins that deform the headgroup layers of the bilayer [27, 64, 96, 107]. Small nanoparticles distort the lipid structure and may affect the integrity of lipid bilayer membranes [68, 69, 105, 106, 122]. Besides surface properties, also particle shape has been found to strongly affect the interaction of small particles with membranes [104]. The formation of a protein corona on the surface of a nanoparticle considerably affects both size and surface properties of the particles [23, 67, 75]. Small polymeric nanoparticles may be unstable and dissolve [90]. The interaction of small nanoparticles with membranes is studied experimentally using optical microscopy [112], electron microscopy [98, 111], and scattering techniques [58, 99]. Atomistic and coarse-grained models can be used to study the interaction of small nanoparticles with membranes using computer simulations [41, 76, 84, 114, 116].

Interaction of Large Particles with Biological Membranes Particles with sizes significantly larger than lipids interact with membranes via wrapping. This encompasses engineered nanoparticles [7, 8, 28, 29, 31, 37–40, 51, 73, 93–95, 119], but also viruses and parasites [26, 30, 78, 113]. Size, shape, surface functionalization, and particle orientation determine the interaction of particles and membranes [21, 29, 45, 89, 115, 118, 124]. An energy gain due to adhesion is opposed by a deformation energy cost for wrapping the membrane around the particle [39]. The adhesion can be mediated by van der Waals interaction or by receptor–ligand bonds [48, 123]. Membrane-mediated and direct interactions may lead to clustering of particles [7, 61, 93, 94]. A passive cytoskeleton below the membrane contributes shear elasticity to the membrane deformation energy [6, 92] and can hinder particle wrapping by the bilayer that it attaches to [54], while an active cytoskeleton can assist particle wrapping [88, 101]. The interaction of large particles with membranes is studied experimentally using optical microscopy [45, 47], electron microscopy [62, 66, 72], atomic force microscopy [83, 110], and scattering techniques [62, 63, 109]. Computer simulations and analytical calculations using coarse-grained and continuum models have been used to study the interaction of large particles with membranes [28, 29, 31, 39, 59, 104].

2 Wrapping by Homogeneous Membranes

Particles that interact with lipid bilayer membranes force the membranes to deform upon particle wrapping (Fig. 2a), which results in deformation energy costs. The adhesion energy gain upon direct contact of the particle with the membrane drives the wrapping process.

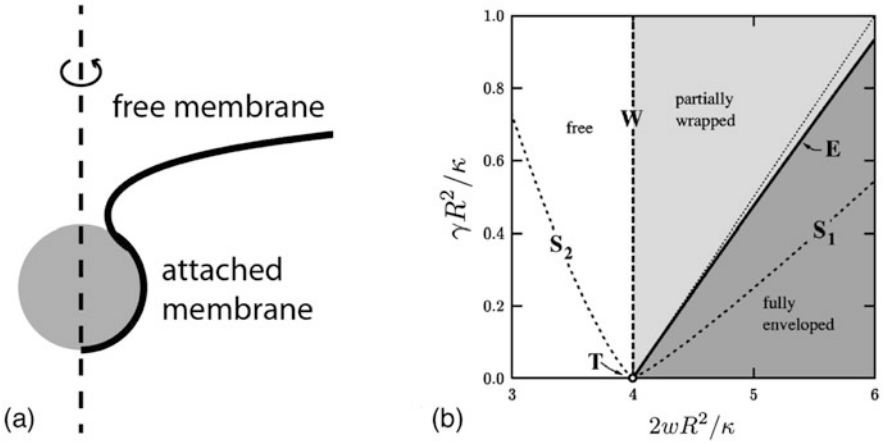

Fig. 2 Wrapping of a spherical nanoparticle of radius R by a membrane with bending rigidity κ and tension γ. The adhesion strength between particle and membrane is w. (**a**) The membrane deforms in a cylindrically symmetric way around the symmetry axis, and the shape can be described by a radial deformation profile. For an infinitely large tensionless membrane, the shape of the free membranes is catenoidal. Reprinted with permission from [32]. CC BY 3.0. (**b**) Wrapping phase diagram for membrane tension and adhesion strength. Nanoparticles are unwrapped for adhesion strengths below $2wR^2/\kappa = 4$, indicated by the thick dashed line (W). They are completely enveloped for adhesion strengths beyond the thick solid line (E). The thin dotted line is the envelopment transition calculated neglecting the deformation energy of the free membrane. The thin dashed lines (S1, S2) describe the spinodals for spontaneous unwrapping (directly to the free state) and for spontaneous envelopment. T indicates the triple point. Reprinted with permission from [37]. Copyright 2004 by the American Physical Society

2.1 Spherical Particles

When particles interact with membranes, both the membrane attached to the particle and the free membrane surrounding the particle get deformed, see Fig. 2a. For spherical particles that attach to an infinitely large tensionless membrane, the free membrane forms a catenoid without deformation energy costs. Spherical particles have the same curvature everywhere on their surface, therefore the deformation energy cost increases linearly with the attached area. The deformation energy cost for wrapping an entire particle with radius R by a membrane with bending rigidity κ and tension γ is $E_{\text{def.}} = 8\pi\kappa + 4\pi R^2\gamma$, and the adhesion energy gain is $E_{\text{adh.}} = -4\pi R^2 w$. The contribution of bending to the deformation energy dominates for particle radii below $R^* = \sqrt{2\kappa/\gamma}$, the contribution of tension for larger particle radii. For values of bending rigidity and tension in the range reported above, $6\,\text{nm} < R^* < 4.5\,\mu\text{m}$.

Particles get wrapped by membranes if the adhesion energy gain exceeds the deformation energy cost, $E_{\text{def.}} + E_{\text{adh.}} \leq 0$. For initially planar membranes, this determines a minimal radius for complete envelopment, $R_{\text{env.}} = \sqrt{2\kappa/(w-\gamma)}$. The minimal radius for binding, $R_{\text{bind.}} = \sqrt{2\kappa/w}$, is independent of the membrane tension [37]. Binding and envelopment transition obtained by these estimates are indicated by the thick dashed line and the thin dotted line in the wrapping phase diagram in Fig. 2b, respectively. While the bending energy is scale invariant, both tension and adhesion contributions to the total energy increase with the surface area of the particle. In the bending-dominated regime, a larger particle therefore gets wrapped easier than a smaller particle. Dimensionless quantities for energies, membrane tension, and adhesion strength,

$$\tilde{E} = E/(\pi\kappa) \qquad \tilde{\gamma} = \gamma R^2/\kappa \qquad \tilde{w} = 2wR^2/\kappa\,, \tag{2}$$

make results universally applicable for various particle sizes. It is obvious from these definitions that for $\gamma = 0$ increasing w is equivalent to increasing R^2.

Figure 2b indicates the wrapping states of particles obtained from energy minimization for various values of w and γ. Below a threshold adhesion strength, particles remain free. The transition from free to partial-wrapped and complete-wrapped states is continuous, and the transition from partial-wrapped to complete-wrapped states is discontinuous. The latter transition is shifted to slightly higher adhesion strengths than those estimated above, because of a local energy minimum for stable partial-wrapped states. The energy barrier between partial-wrapped and complete-wrapped states results in spinodals that delimit the regimes where particles spontaneously wrap and unwrap. While wrapping occurs via stable partial-wrapped states, spontaneous unwrapping occurs directly to the free state.

2.2 *Nonspherical Particles*

Particle shape is a critical parameter for drug delivery [44]; for example, higher specificity has been reported for nonspherical antibody-displaying nanoparticles compared with spherical particles [11]. Engineered nanoparticles with a variety of shapes can be fabricated, see Fig. 3. Furthermore, viruses can have very different shapes, e.g., elongated filoviruses and bullet-shaped rhabdoviruses [49, 113], and, for example, the malaria parasite is egg-shaped [30]. Nonspherical particles at homogeneous membranes show a much richer wrapping behavior compared with spherical particles, because the curvature of their surface is not homogeneous. The local bending energy cost is proportional to the squared mean curvature of the membrane, while the adhesion energy gain is independent of the shape of the membrane. Thus, energy barriers for wrapping are associated with highly curved regions on the particle surface, which stabilizes partial-wrapped states. For example, for wrapping fractions below 50 %, ellipsoidal particles have partial-wrapped states with their long axis parallel to the membrane that avoid the strong membrane

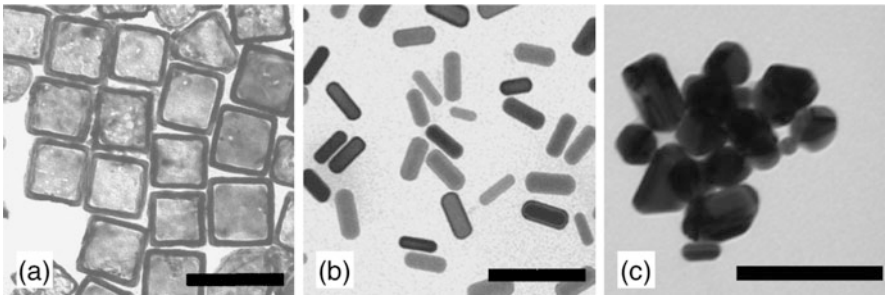

Fig. 3 Examples for engineered nanoparticles: (**a**) Cube-like and (**b**) rod-like gold nanoparticles. Reprinted by permission from Macmillan Publishers Ltd: Nat. Nanotech., [22], Copyright © 2011. (**c**) Silver nanoparticles with irregular shapes. Reprinted with permission from [61]. OA CC BY 4.0. The length of the scale bars corresponds to 100 nm

deformations at the highly curved tips of the particle [31]. Similarly, for cube-like and rod-like particles highly curved ridges constitute energy barriers [29]. In contrast, locally planar parts of the particle surface, such as the faces of a cube, readily attach to a planar membrane at infinitely small adhesion strengths.

Nonspherical particle shapes can be described analytically using $(x/a)^n + (y/a)^n + (z/b)^n = 1$ for cube-like particles and $[(x^2 + y^2)/a^2]^{n/2} + (z/b)^n = 1$ for rod-like, "superegg" particles. In both expressions, $a = b$ and $n = 2$ gives a sphere; a superegg with $a \neq b$ and $n = 2$ is an ellipsoid. The deformation energy can be calculated numerically using triangulated membranes [14, 50], where the surface is constructed by small triangles. The dihedral angle between adjacent triangles is used to calculate the bending energy; the total area of all triangles couples to the membrane tension. Figure 4a–c shows a wrapping diagram and snapshots for stable, partial-wrapped states for a Hauser's cube-shaped particle, described by $(x/a)^6 + (y/a)^6 + (z/a)^6 = 1$. We use dimensionless parameters $\tilde{\gamma} = \gamma a^2/\kappa$ and $\bar{w} = wA/(2\pi\kappa)$, where A is the particle surface area. The particle attaches at vanishing adhesion strength to one of the flat faces. In this shallow-wrapped state, the membrane binds to approximately $1/6$ of the particle's surface area. In order to transit to the deep-wrapped state with a wrapping fraction of $5/6$, an energy barrier because of the highly bent edges of the particle has to be overcome; the same applies for the transition from the deep-wrapped state to the complete wrapped state. Because of the energy barriers, these transitions are discontinuous already for tensionless membranes. In addition to a globally stable state with the lowest energy, the system may therefore also be found in a metastable state. Qualitatively similar wrapping behavior is observed for other nonspherical particles. In general, a nonspherical particle shape stabilizes partial-wrapped states.

While the binding transition of the particle is always continuous, the other transitions between wrapping states are often associated with energy barriers and are thus discontinuous. For elongated particles, also the orientation of the particle with respect to the membrane varies with the wrapping state. For shallow-wrapped

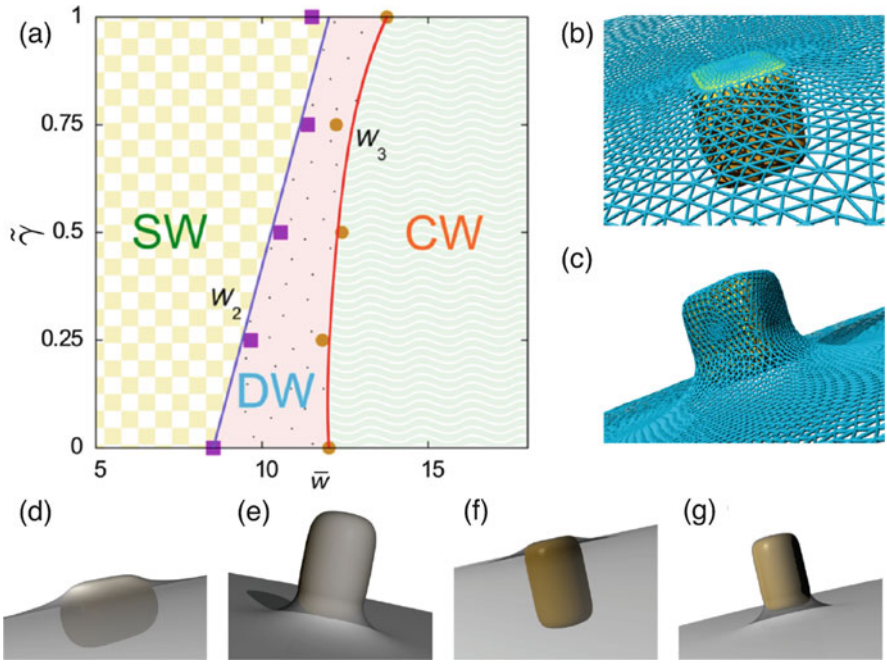

Fig. 4 Wrapping of cube-like and rod-like nanoparticles. (**a**) Phase diagram for wrapping of Hauser's cube for membrane tension $\tilde{\gamma}$ and adhesion strength $\bar{w}$; the parameters are given in dimensionless form. We find a shallow-wrapped (SW), a deep-wrapped (DW), and a complete-wrapped (CW) state, separated by two discontinuous wrapping transitions, W_2 and W_3. (**b**), (**c**): Membrane deformation for wrapping of Hauser's cube. The network of edges and triangles describes the membrane shape and is used for the numerical calculation of the curvature energy. Membrane conformations are shown at fixed tension $\tilde{\gamma} = 0.50$ for two corresponding states at the W_2 phase boundary: (**b**) a shallow-wrapped state with approximately 10% of particle wrapped, and (**c**) a deep-wrapped state with a wrapping fraction of approximately 80%. (**d**)–(**g**) Membrane-particle conformations for rod-like nanoparticles with (**d**) $n = 4$ and $b/a = 1.5$ (SW), (**e**) $n = 4$ and $b/a = 1.5$ (DW), (**f**) $n = 6$ and $b/a = 1.5$ (SW), and (**g**) $n = 6$ and $b/a = 1.5$ (DW). Adapted with permission from [29]. Copyright (2014) American Chemical Society

states, particles are mostly oriented with their long axis parallel to the membrane, the so-called submarine orientation, while for deep-wrapped states particles are oriented with their long axis perpendicular to the membrane, the so-called rocket orientation. This behavior can again be rationalized by the requirement to maximize the adhered membrane area while avoiding highly curved regions of the particle. A point of caveat for comparing the wrapping behavior of particles with different shapes quantitatively is that particle size also has to be taken into account. Although the bending energy is scale-independent, the tension and adhesion contributions to the total energy are not. Therefore, when comparing, for instance, two rod-like particles with different aspect ratios, it is essential to specify whether particle volume, surface area, or the length of the small axis is fixed [29]. Table 1 qualitatively summarizes

Table 1 Shape dependence of particle wrapping, based on [28, 31, 37] and this work

Particle shape	Membrane	Binding transition	Shallow-wrapped state	Deep-wrapping transition	Deep-wrapped state	Envelopment transition
Spherical	κ	Cont., for $w = 2\kappa/R^2$	–	–	–	$\equiv$ binding
Spherical	κ and γ	Cont., for $w = 2\kappa/R^2$	Yes	–	–	Discont.
Ellipsoidal	κ, κ and γ	Cont., indep. of γ	Yes, submarine	Discont., reorient.	Yes, rocket	Cont.
Ellipsoidal[a]	κ, κ and γ	Cont., indep. of γ	Yes, submarine	–	–	Discont.
Cube-like	κ, κ and γ	At vanishing w	Yes	Discont.	Yes	Discont.
Sphero-cylinder	κ, κ and γ	At vanishing w, rocket	Yes, submarine	Discont., reorient.	Yes, rocket	Discont.
Rod-like	κ, κ and γ	At vanishing w, rocket	Yes, submarine	Discont., reorient.	Yes, rocket	Discont.
Rod-like[a]	κ, κ and γ	At vanishing w, rocket	Yes, submarine	–	–	Discont.
Rod-like[b]	κ, κ and γ	At vanishing w, rocket	Yes, rocket	Discont.	Yes, rocket	Discont.

The membrane can be characterized by bending rigidity only, "κ", or by bending rigidity and membrane tension, "κ and γ"; the binding transition can occur at finite or vanishing adhesion strength w; the particle can be in submarine or rocket orientation; transitions can be continuous (cont.) or discontinuous (discont.) and may involve reorientation (reorient.). The binding transition for ellipsoids is independent of the membrane tension and is given in [28, 31]. Reprinted with permission from [29]. Copyright (2014) American Chemical Society

[a]Fast wrapping at high adhesion strength, such that a bound ellipsoid cannot reorient to rocket orientation

[b]Rocket mode for supereggs with blunt tips and small aspect ratio (e.g., $n = 4$ and $b/a = 1.5$)

the wrapping behavior for various shapes of the particle and curvature-elastic properties of the membrane.

The role of edge curvature for wrapping nonspherical particles is illustrated in Fig. 5. A spherical particle at a tensionless membrane directly transits from the free to the complete-wrapped state. Ellipsoidal particles experience an energy barrier between the shallow-wrapped state in submarine orientation and the deep-wrapped/complete-wrapped state that depends on the curvature of the tips and therefore on the aspect ratio. For a rod-like particle, aspect ratio and edge curvature are independent of each other. In the shallow-wrapped state, a particle is found in rocket ($b/a = 1$) or submarine ($b/a = 2$) orientation. The extent of the partial-wrapped regime increases with edge curvature, and the transitions to the deep-wrapped state and to the complete-wrapped state both shift to higher values of the adhesion strength. Therefore, not only size and aspect ratio of a particle, but also local curvature distribution and, e.g., surface roughness crucially influence the wrapping behavior.

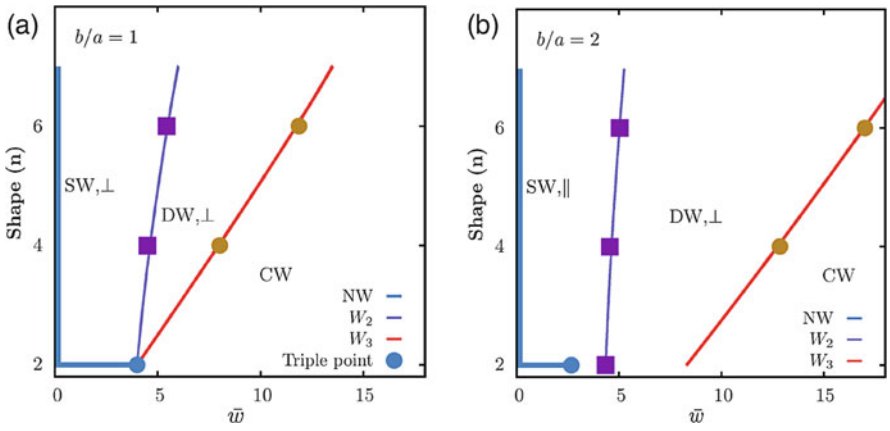

Fig. 5 Role of edge curvature (characterized by n) on the wrapping behavior of a tensionless membrane for rod-like nanoparticles with fixed aspect ratios, (**a**) $b/a = 1$ and (**b**) $b/a = 2$. The particle orientation in the shallow-wrapped (SW) and the deep-wrapped (DW) states is indicated by the symbols $\perp$ and $\parallel$, corresponding to rocket and submarine orientation, respectively. Non-wrapped (NW) states are marked by light-blue lines, and W_1 and W_2 indicate the transitions between shallow-wrapped and deep-wrapped states, and between deep-wrapped and complete-wrapped states, respectively. Reprinted with permission from [29]. Copyright (2014) American Chemical Society

2.3 *Deformable Particles*

Macrophages preferentially engulf rigid objects [13]. Soft microgel particles in the hydrophilic swollen state have been shown to adsorb densely on giant unilamellar vesicles; the same particles in the more hydrophobic collapsed state remain attached, but partially desorb from the membrane and self-organize in domains [73]. Both observations indicate that particle wrapping is also affected by particle deformability. When soft particles get wrapped by lipid bilayer membranes, for partial-wrapped states not only the membrane but also the particle deforms, see Fig. 6a, b. Therefore in a passive system, a soft particle that attaches to a planar membrane assumes an oblate shape, and the deformation of the planar membrane is reduced compared to a hard particle of the same size. Wrapping of a lipid vesicle or a thin elastic capsule with initial radius R by a lipid membrane can serve as model system for wrapping of a soft particle [117, 119, 121]. The total energy for a vesicle wrapped by an initially flat membrane is [119]

$$\mathscr{H} = \sum_{i=1,2,3} \int_{S_i} dS_i \left[2\kappa_i H^2 + \bar{\kappa}_i K \right] + pV_\mathrm{v} + \Gamma A_\mathrm{v} + \gamma A_\mathrm{f} - wA_\mathrm{ad} \,, \qquad (3)$$

where $i = 1$ denotes the vesicle membrane, $i = 2$ the initially planar membrane, and $i = 3$ the double bilayer formed by vesicle and planar membrane. Thus, $\kappa_3 = \kappa_1 + \kappa_2$ and $\bar{\kappa}_3 = \bar{\kappa}_1 + \bar{\kappa}_2$. In addition, p, Γ, γ, and w characterize the energy change

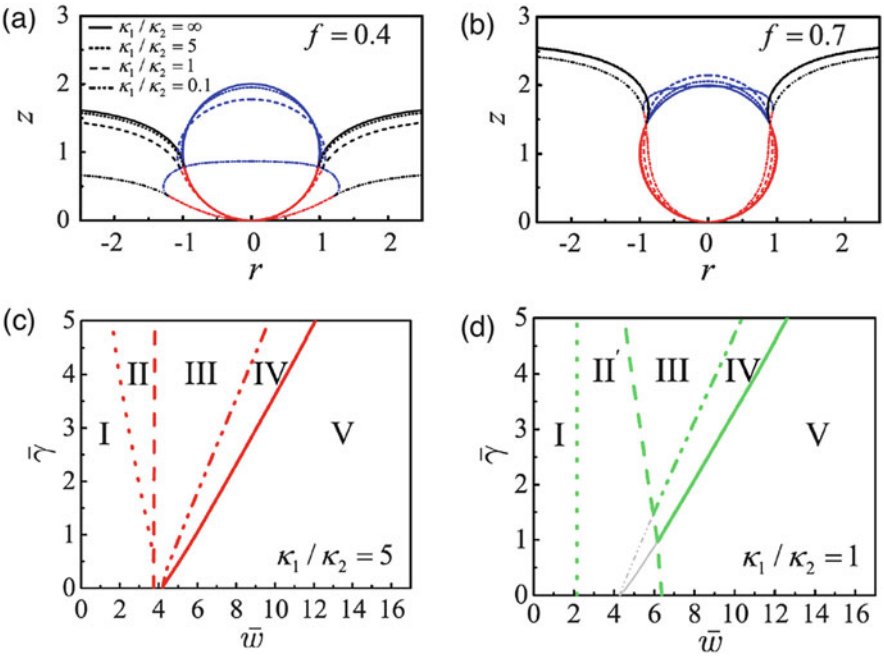

Fig. 6 Wrapping of vesicles by initially flat membranes. (**a**)–(**b**) Vesicle shapes for partial-wrapped states with wrapping fractions $f = 0.4$ and $f = 0.7$ for various ratios of the bending rigidity of vesicle and initially flat membrane, κ_1/κ_2. (**c**)–(**d**) Wrapping phase diagrams for pressure $p = 0$ with respect to the dimensionless adhesion strengths $\bar{w} = 2wR^2/\kappa_2$ and surface tension $\bar{\gamma} = 2\gamma R^2/\kappa_2$ at different values of the rigidity ratio κ_1/κ_2: (I) stable non-wrapped state, (II) stable non-wrapped and metastable partial-wrapped state, (II') stable partial-wrapped and unstable non-wrapped state, (III) stable partial-wrapped state and metastable complete-wrapped state, (IV) stable complete-wrapped state and metastable partial-wrapped state, and (V) stable complete-wrapped state. Reprinted with permission from [119]. Copyright 2011 by the American Physical Society

upon changes of volume V_v and area A_v of the vesicle, area A_f of the initially flat membrane, and the contact area A_{ad} between vesicle and membrane, respectively.

Phase diagrams for wrapping of soft nanoparticles with different ratios between the stiffnesses of the vesicle membrane and the membrane that wraps the vesicle, κ_1/κ_2, are shown in Fig. 6c, d. For stiff vesicles, the wrapping phase diagram in Fig. 6c is very similar to the wrapping phase diagram for hard spherical nanoparticles in Fig. 2b. For soft vesicles, the phase boundary between non-wrapped and partial-wrapped states is shifted to smaller adhesion strengths, see Fig. 6d. The regime with stable non-wrapped states and metastable partial-wrapped states is replaced by a regime with stable partial-wrapped and unstable non-wrapped states, which also partially extends into the regime of stable complete-wrapped states for hard particles. Soft nanoparticles therefore attach much more readily to membranes, while at the same time the transition to the complete-wrapped state shifts to higher adhesion strengths.

2.4 Dynamics

The dynamics of particle wrapping is determined by the typical timescales of the relevant processes, such as membrane deformation and—for complex membranes—receptor diffusion and potentially deformation or remodeling of the cytoskeleton. Molecular dynamics simulations for nanoparticles that interact with initially flat lipid bilayer membranes allow to follow a typical wrapping process in time [59, 104]. After the initial contact between nanoparticle and membrane, the size of the deformed membrane patch around the particles increases; it is largest for about half-wrapped nanoparticles. Towards the end of the wrapping process, the bent membrane attached to the particle is connected to the flat region surrounding the particle only by a small neck. Formation of a defect in the neck leads to separation of bent and flat membrane and completes the wrapping process.

Dynamics is particularly interesting for nonspherical particles that attach to lipid bilayer membranes. While the stable orientation for elongated particles at small wrapping fraction is (usually) the submarine orientation with the long axis parallel to the membrane, for high wrapping fraction the rocket orientation with the long axis perpendicular to the membrane corresponds to the lowest energy [29]. Coarse-grained molecular dynamics simulations allow to follow the orientational changes that elongated nanoparticles undergo during wrapping [59, 104]. A local free energy analysis and incremental changes of the nanoparticle orientation in the direction of lowest energy allow to predict a wrapping pathway, see Fig. 7. The corresponding curvature energy landscapes are plotted using color density plots. A sphero-cylindrical nanoparticle that is initially in the unfavorable rocket orientation first reorients towards submarine orientation. Although energetically most favorable until half-wrapping, the particle may never actually reach submarine orientation. Beyond half-wrapping, the particle turns back to the then favorable

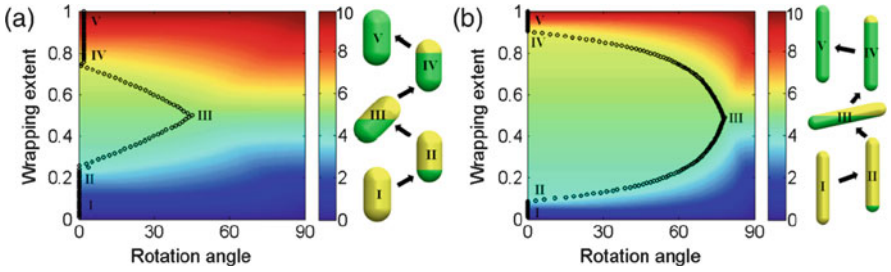

Fig. 7 Endocytic pathways for nanoparticles with aspect ratios (**a**) 2 and (**b**) 5.5 predicted by local energetics. The sphero-cylindrical nanoparticles take a general laying-down-then-standing-up sequence during endocytosis. The contour maps plot the curvature energy level in the plane of rotation angle and wrapping extent. The turning points (I–V) along the endocytic pathways predicted by local free-energy analysis are schematically shown in each subfigure, where the green-shaded areas are wrapped, while yellow-shaded areas are naked. Reprinted with permission from [59]. Copyright (2013) American Chemical Society

rocket orientation, in agreement with the energetics discussed in Sect. 2.2. For very fast uptake, reorientation may be suppressed and an ellipsoidal particle may, for example, be taken up completely in submarine orientation [31].

3 Wrapping by Complex Membranes

Many biological membranes contain a variety of lipids and proteins and are much more complex than the model membranes that have been discussed so far [91]. These different components can interact with particles and pathogens and may either be randomly distributed as suggested by the fluid mosaic model or aggregated already before the interaction with particles in lipid rafts [77]. Furthermore, a cortical cytoskeleton may rigidify the membrane by adding shear elasticity [6, 53], slow down diffusion within the membrane [5], and alter distribution of lipids and proteins [42].

3.1 Two-Component Membranes with Domains

Particle adhesion has been found experimentally to depend on lipid composition and membrane structure: small particles with $R < 100\,\mathrm{nm}$ have been observed to attach to the liquid-ordered phase, larger particles attach to the liquid-disordered phase [52]. Computer simulations for a particle that is attached to a lipid raft show that the presence of the domain boundary facilitates particle detachment from the membrane after complete wrapping [97]. Membranes where two or more phases with different lipid compositions coexist can be described by a set of elastic parameters for each domain and a line tension at the domain boundary. Domain formation alone can induce budding [12, 70], therefore domains can assist particle wrapping. The effect of lipid phase segregation on the interaction of particles with membranes can be investigated using the Hamiltonian:

$$\mathscr{H} = \sum_{i=1,2} \left\{ \int_{S_i} dS_i \left[\gamma_i + 2\kappa_i (H - c_{0,i})^2 + \bar{\kappa}_i K \right] + \gamma_\ell \int_{\ell_c} d\ell - w_i \int_{S_{\mathrm{ad,i}}} dS_i \right\}, \tag{4}$$

where the sum adds the integrals over a domain and its surrounding, see Fig. 8a. The line tension γ_ℓ arises at the boundary where the phases are in contact, and it might be very small if hybrid lipids with one saturated and one partially unsaturated chain act as line-active component [15]. The value of $\bar{\kappa}$ is not well known in many cases, because the Gaussian saddle-splay modulus only contributes to the energy of the membrane if it is inhomogeneous or if topology changes of the membrane are observed. We neglect this contribution in the following discussion, the contribution at the domain boundary might be thought of as redefined line tension.

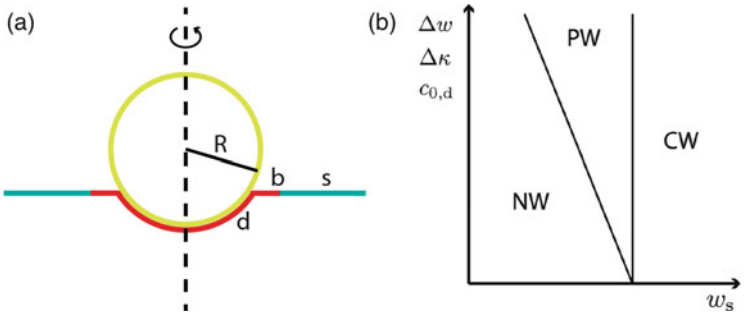

Fig. 8 Particle wrapping by multicomponent membranes with strong segregation. (**a**) Membrane with domain size smaller than the particle surface area partially wrapped around the particle (d: domain area, s: surrounding membrane, and b: domain boundary). (**b**) Wrapping phase diagrams for a particle that preferentially adheres to a domain that is smaller than the surface area of the particle (NW: non-wrapped particle, PW: partial-wrapped particle, and CW: complete-wrapped particle). The phases are sketched for the adhesion strength of the surrounding membrane w_s and either the difference of the adhesion strengths Δw, the difference of the bending rigidities $\Delta\kappa$, or the spontaneous curvature $c_{0,\mathrm{d}}$ of the membrane that forms the domain. All other parameters are kept constant. Calculated using the model in (**a**)

Figure 8b shows a phase diagram for particles that interact with a domain in a tensionless, phase-separated membrane with vanishing line tension at the domain boundary. If the domain is larger than the surface area of the particle, the wrapping behavior is expected to be similar to a homogeneous membrane. If the domain is too small to cover the entire surface area of the particle, the change of curvature-elastic constants and adhesion strength is reflected in the wrapping phase diagrams. The diagram shows wrapping phases for particles that adhere to a domain with adhesion strength $w_\mathrm{d} \geq w_\mathrm{s}$, where w_s is the adhesion strength between the particle and the surrounding membrane. Stable partial-wrapped states occur when the w_d is large enough for wrapping, but w_s is too small. The phases are plotted for w_s and $\Delta w = w_\mathrm{d} - w_\mathrm{s}$. Analogous to an increased adhesion strength, stable partial-wrapped states are found if the bending rigidity of the membrane that forms the domain is smaller than the bending rigidity of the surrounding membrane, $\Delta\kappa = \kappa_\mathrm{s} - \kappa_\mathrm{d} > 0$, and if the membrane of the domain has a preferable spontaneous curvature $c_{0,\mathrm{d}}$. A finite line tension for the boundary of a preexisting domain also assists wrapping, because the length of the domain boundary decreases with increasing wrapping fraction of the particle.

3.2 Receptor–Ligand Bond-Mediated Wrapping

The interaction of particles with multicomponent membranes in a single phase cannot be described by domains with different curvature-elastic parameters and adhesion strengths as discussed in Sect. 3.1. Here, the presence of the nanoparticle

can induce segregation of the components, such as aggregation of receptors in the adhered region. Experimental data indicates the importance of receptor-mediated nanoparticle wrapping. For example, particles that are half-coated with ligands are endocytosed in steps [47]. In a first step, a membrane cup forms on the ligand-coated surface and afterwards the endocytic process stalls. Only in a second step, the ligand-absent hemisphere is wrapped. Furthermore, experiments for nanoparticle uptake by cells reveal a preferred particle radius of about 25 nm [20, 21, 81], while calculations with a homogeneous adhesion strength between particle and membrane predict that the larger the nanoparticle the easier it gets wrapped. This has triggered theoretical studies on receptor-mediated endocytosis using kinetic [9, 34, 35, 48] and free-energy approaches [33, 120] that both predict an optimal radius for uptake close to the experimentally observed radius.

Receptor-mediated adhesion is a natural choice to model the adhesive interaction in computer simulations, because nanoparticles are often modeled by an assembly of beads [59, 104]. Figure 9a shows wrapping for a nanoparticle with ligand coverages of 20% and 80% and receptor–ligand bond energies $\epsilon = 2\,k_{\mathrm{B}}T$ and $\epsilon = 8\,k_{\mathrm{B}}T$. A bound nanoparticle is observed for small bond energy and small ligand coverage, a partial-wrapped nanoparticle is observed for small bond energy and high ligand coverage or for high bond energy and low ligand coverage, and a complete-wrapped nanoparticle is observed for high ligand coverage and high bond energy. Analogous to the competition of adhesion energy and bond energy, for homogeneous adhesion strength the nanoparticles get wrapped only if the adhesion energy gain exceeds the deformation energy cost (this estimation neglects an energy minimum for partial-

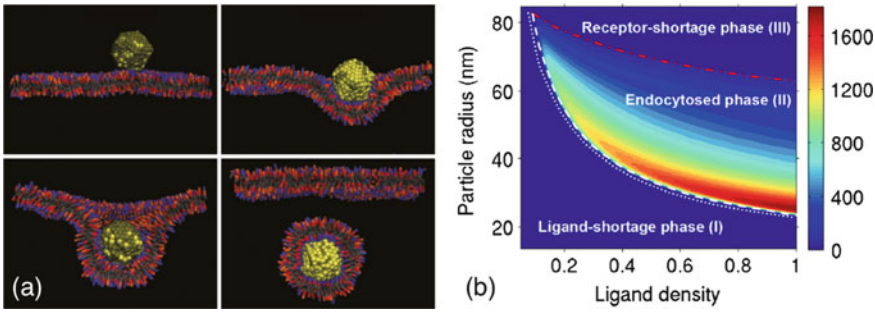

Fig. 9 Particle wrapping by multicomponent membranes with weak segregation. (**a**) Receptor-mediated wrapping for a spherical nanoparticle interacting with a membrane. Binding, partial, and complete wrapping are observed depending on ligand coverage and receptor–ligand bond energy. Color coding: nanoparticle, yellow beads are ligands and gray beads are purely repulsive; membrane, blue beads are membrane receptors, orange are headgroups, and gray and orange are tail beads. Adapted with permission from [104]. Copyright (2011) American Chemical Society. (**b**) The phase diagram shows the cellular uptake for various particle sizes and ligand densities. The dotted line represents the theoretical lower bound $R = \sqrt{2\kappa/\epsilon}a_{\mathrm{r}}$. The color bar indicates the level of cellular uptake. The endocytosed phase (II) is separated from the ligand-shortage phase (I) and the receptor-shortage phase (III) by the dashed and the dashed-dotted line. Reprinted with permission from [120]. Copyright 2010 by the American Physical Society

wrapped states). A minimal particle radius is given by $\epsilon/a_r^2 > 2\kappa/R^2$, where a_r is the area per receptor.

For a given wrapping fraction of the nanoparticle, the free energy for the receptors on the membrane is

$$F = -N_b\epsilon - k_B T \ln\left[\binom{S_b}{N_b}\binom{S_f}{N_f}\right]. \tag{5}$$

Here, we assume the ligands to be regularly distributed and fixed on the particle. The receptor entropy is calculated for a membrane that is discretized into sites. S_b and S_f are the numbers of available sites on the bound and unbound region of the membrane, and N_b and N_f the numbers of bound and free receptors. The first term represents the total bond energy and the second term represents the contribution of the receptor entropy to the free energy. This is a simplified model that highlights the interplay of bond energy and entropy of the receptors. A more complete model for receptor-mediated adhesion accounts in addition for the entropy of the differently wrapped nanoparticles, the enthalpy change by taking nanoparticles out of the solution, and the membrane deformation energy [120]. Figure 9b quantifies cellular uptake for a membrane with bending rigidity and tension. Three different wrapping regimes are found: (1) a ligand-shortage phase where $\epsilon/a_r^2 < 2\kappa/R^2$, (2) an endocytosed phase where the nanoparticle gets wrapped, and (3) a receptor-shortage phase where both membrane tension and receptor entropy prevent wrapping.

Extensions of the basic model for receptor-mediated adhesion of single particles allow to study of further aspects of related systems. For example, taking into account mutual attraction of nanoparticles during cellular uptake leads to distributions for uptake as function of nanoparticle size that agree better with the experimental data than single-particle calculations [19]. In biological systems with high salt concentrations and strong electrostatic screening, charged membranes that interact with charges on the nanoparticle show a similar dependence of the energy of the system on the wrapping fraction as found for receptor-mediated wrapping [46]. In particular, frustrated endocytosis with partial-wrapped states is observed for lack of charges on the membrane. Receptor-like models can also be used to understand the role of curved proteins for wrapping, where the energy gain for the proteins in the membrane adhered to the particle with favorable curvature competes with the loss of entropy for protein aggregation [2, 79]. Finally, viral budding from and entry into host cells is a receptor-mediated process [80, 102].

4 Many-Particle Interactions

Many-particle interactions significantly alter the interaction of nanoparticles with membranes. For example, single nanoparticles are too small to be phagocytosed, but aggregates may enter the cell via this pathway [16]. For dosage-dependent effects, also membrane-mediated interaction is an important player in addition to

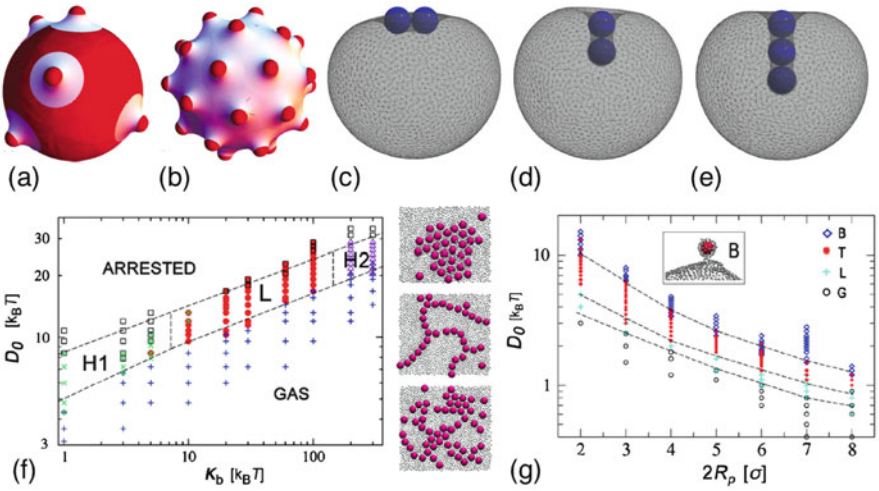

Fig. 10 Membrane-mediated interaction. (**a**)–(**b**) Inclusions, indicated by small red caps, on a vesicle. White catenoidal deformations with vanishing bending energy form around the inclusions. An inclusion-decorated vesicle with vanishing bending energy cost at optimal inclusion density. Reprinted with permission from [4]. Copyright 2009 by the American Physical Society. (**c**)–(**e**) Nanoparticles attached to a vesicle aggregate, tubes form for sufficiently small reduced volume of the vesicle, such that enough area is available to allow for this deformation. Reprinted with permission from [7]. Copyright 2012 by the American Physical Society. (**f**) Phase diagram for nanoparticle self-assembly in terms of membrane bending rigidity $K_b = 2\sqrt{3}\kappa$ [50] and particle binding strength D_0 that is proportional to the adhesion strength w. The snapshots show typical aggregates in H1, L, and H2 phase (top to bottom). Reprinted with permission from [93]. Copyright 2012 by the American Physical Society. (**g**) Phase diagram in terms of nanoparticle radius R_p (in units of the radius of the beads that are used to represent the membrane in the simulations) and D_0: gaseous phase G, linear aggregation L, tube formation (T), and single-particle bud formation B. Reprinted with permission from [94]. Copyright 2012 by the American Physical Society

direct interaction between nanoparticles. We first discuss the interaction of curved inclusions: while two small spherical-cap inclusions—where the cap is only a small part of the entire sphere—interact repulsively, for large spherical caps attraction is observed [86, 87]; furthermore, many inclusions aggregate and induce bud formation [3, 4, 87]. Figure 10a, b shows catenoidal membrane deformations around inclusions that reduce the total bending energy of an inclusion-decorated vesicle compared with a bare vesicle. The bending energy of the inclusion-decorated vesicle vanishes at optimal inclusion density, while an energetic cost arises from the same number of inclusions at maximal mutual distance on a planar membrane of finite size. Thus, vesicle curvature screens the membrane-mediated repulsion between inclusions.

The membrane-mediated many-particle interactions that have been studied so far are always attractive. For instance, two particles form a dimer that switches from a linear aggregate on the membrane to a tubule for increasing wrapping fraction [7, 94], see also the discussion on submarine and rocket orientation of elongated

particles in Sect. 2.2. The wrapping fraction of the particle can be tuned by adjusting the reduced volume of the vesicle, $v = V/V_{\mathrm{sph}}$, where V is its actual volume and V_{sph} is the volume of a spherical vesicle with the same membrane area. Small reduced volumes allow more than two particles to join a tube. The energetic gain of tubular assemblies compared with single, complete-wrapped particles strongly depends on the range of the particle–membrane interaction potential ρ; for example, the energy gain is about $5\,\kappa$ for $\rho/R = 0.2$ [85], because the curvature energy decreases for a tube-like arrangement of nanoparticles, but the adhesion energy hardly increases due to the finite potential range.

Figure 10f shows a phase diagram for many nanoparticles on a membrane for different values of κ and particle binding strength D_0 [93]. For small bending rigidities, partial-wrapped particles form a hexagonal cluster phase where the membrane penetrates inbetween the particles. For high bending rigidities, partial-wrapped particles are barely attached to the membrane; they deform the membrane only weakly and therefore also interact only weakly. Linear aggregates are observed inbetween both phases for biologically relevant bending rigidities $10\,k_{\mathrm{B}}T < \kappa < 100\,k_{\mathrm{B}}T$. Whereas the deformation energy cost prefers a hexagonal cluster, the higher adhesion energy gain leads to formation of linear clusters [93]. Linear aggregates have also been observed in experiments where colloidal particles were bound to giant unilamellar vesicles (GUVs) [65]. In computer simulations at high adhesion strengths, the particles are found in an arrested phase; this can either be single-particle buds or tubular aggregates [94], see Fig. 10g. Tubule formation has been observed experimentally, for instance, for the interaction of viruses with cells and GUVs [43].

5 Pathogens and Other Active Biological Systems

Phagocytosis—a feeding mechanism or an immune response to foreign objects of cells—and entry or exit of parasites involve active biological processes. For example, mammalian cells form actin protrusions to interact with their immediate environment; membrane reservoirs and clustering of receptors and signaling molecules can help to sculpture the plasma membrane into different shapes. The malaria parasite is equipped with motor complexes that can assist invasion into red blood cells.

5.1 Invasion of the Malaria Parasite into Erythrocytes

Malaria is a deadly disease that affects several hundred million people every year around the world. One of the crucial stages of infection is the blood stage, where the merozoites invade red blood cells [25]. A merozoite has an asymmetric egg-like shape with a total surface area of $8\,\mu\mathrm{m}^2$ and a width/length ratio of 0.71. Merozoites

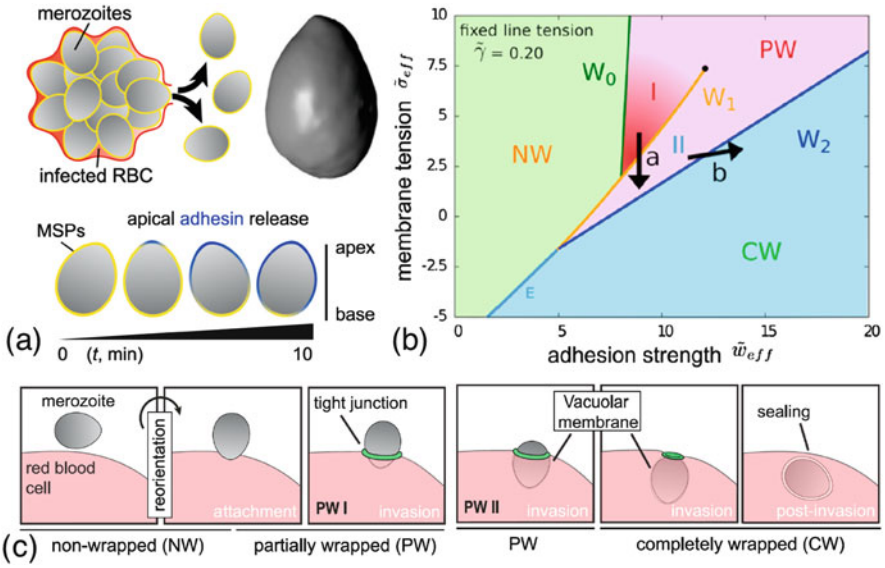

Fig. 11 Membrane-wrapping contributions to malaria parasite invasion of the human erythrocyte. (**a**) Malaria egress from an infected erythrocyte and an isosurface of a merozoite obtained from cryo X-ray imaging. Merozoites are infectious for about 10 min, during which an adhesin gradient may develop. (**b**) Wrapping phase diagram for a tip-first-oriented merozoite for adhesion strength and membrane tension at fixed reduced line tension $\tilde{\gamma} = 0.2$: (**c**) Schematic representation depicting different wrapping phases of the merozoite from reorientation through to invasion and post-invasion. Reprinted with permission from [30]. CC BY 4.0

approach the erythrocyte surface in a random orientation and then quickly undergo reorientation with the pointed apical end towards the membrane. This reorientation can be triggered by an adhesive gradient on the merozoite surface, see Fig. 11a. Next, the merozoite invades the erythrocyte within several minutes by traversing through the partial-wrapped states PW I and PW II, see Fig. 11b.

Phase diagrams for wrapping the parasite with erythrocyte membrane highlight the interplay of membrane curvature elasticity and tension, parasite shape and adhesion energy, and line tension where the membrane detaches from the parasite (that possibly originates from the cytoskeleton of the erythrocyte) [30]. Wrapping phase diagrams can be calculated along the same lines as described in Sect. 2. The states in the phase diagram for a tip-first-oriented merozoite and a fixed line tension in Fig. 11b correspond to the sketches in Fig. 11c: non-wrapped (NW), partial-wrapped with small wrapping fraction (PW I), partial-wrapped with high wrapping fraction (PW II), and complete-wrapped (CW). The transition W_0 between the non-wrapped and the partial-wrapped state is continuous, whereas the transitions W_1, W_2, and E are discontinuous. At a critical membrane tension, the energy barrier between the two partial-wrapped states vanishes and W_1 ends at a critical point. The arrows in Fig. 11b indicate active biological processes during invasion: **a** secretion

of unstructured membrane by the merozoite, and **b** aggregation or secretion of membrane components with favorable spontaneous curvature.

Wrapping-energy calculations provide a systematic understanding for passive energetic contributions to the invasion process and can help to quantify the effect of various active biological processes. (1) A gradient of adhesive strength can lead to tip-first orientation of the parasite, the crucial first step of the invasion process. (2) Parasite-stimulated reorganization of the erythrocyte cytoskeleton and release of parasite-derived membrane area may affect elastic properties of the host-cell membrane, such as tension and spontaneous curvature and thereby facilitate wrapping. (3) Parasite actomyosin motor contributions can help to overcome energetic barriers and to transition from metastable partial-wrapped to stable complete-wrapped states. Combining these biophysical insights with a parasitological framework, drawing on a broad foundation of molecular and cellular evidence, it is proposed that invasion is achieved via a balance between parasite and host cell contributions. These findings lay the foundations for identifying mechanisms related to the host cell membrane that might be targeted in malaria treatment.

5.2 Active Invasion Mechanisms During Phagocytosis

Phagocytosis involves complex physiological mechanisms by which eukaryotic cells ingest nutrients and immune cells eliminate pathogenic particles or dead biological material. While particles with sizes below 500 nm are internalized via receptor-mediated endocytosis, particles with sizes larger than 1 μm are internalized through a phagocytic process [36]. Here, cells employ active mechanochemical processes, such as cytoskeletal reorganization. Actin–myosin rings or phagocytic cups, specific or unspecific adhesion mediated via receptor–ligand bonds, and dynamical regulation of membrane tension assist to sculpture the plasma membrane into a phagosome. Experiments demonstrate that local particle shape, not overall particle size, plays a decisive role in initiating phagocytosis [17, 74]. For instance, macrophages that attach to a flat side of an oblate ellipsoidal particle spread on one side of the particle, but no formation of an actin ring and no phagocytosis are observed. Figure 12a shows representative scanning electron micrographs and fluorescent micrographs with actin staining for cells that interact with polystyrene particles of different shapes. The fluorescent micrographs reveal remodeling of the cytoskeleton to form ring-like and cup-like structures. The experiments suggest that cells are not able to detect macroscopic properties, such as volume, until phagocytosis is complete. However, the size of the particle could prevent the cell from successfully completing internalization.

Cellular uptake of large spherical particles by phagocytosis occurs in two distinct phases, see Fig. 12b. During a first, slow engulfment phase, wrapping is achieved by actin-rich protrusions. Receptor-mediated interactions drive the wrapping process, such that for specific adhesion the efficiency can be increased by higher receptor densities [17, 47]. During a second, fast envelopment phase,

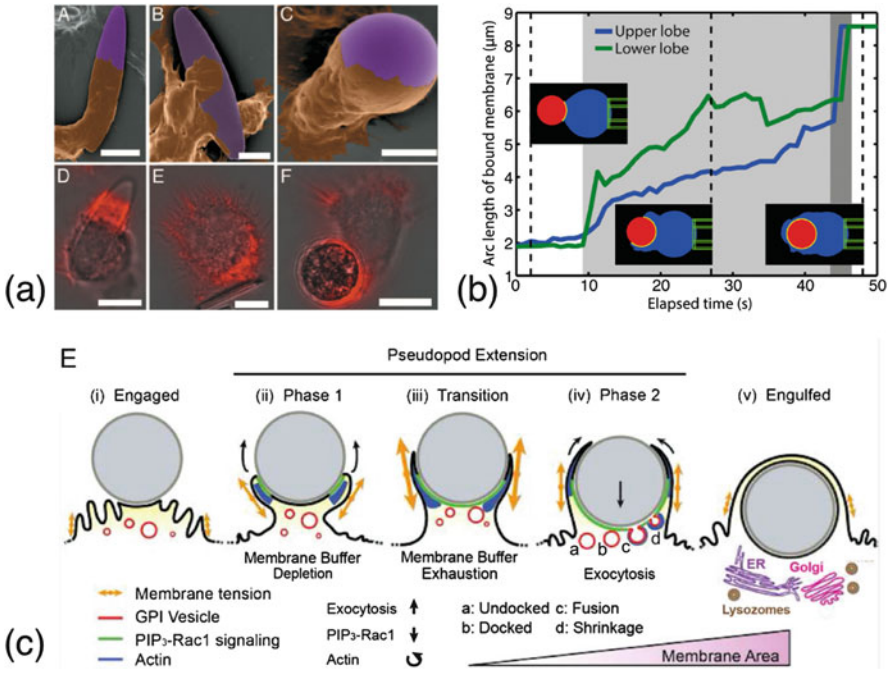

Fig. 12 Phagocytosis. (**a**) Micrographs of cells and opsonized particles, colored brown and purple, respectively, and overlays of bright-field and fluorescent images after fixing the cells and staining for polymerized actin with rhodamine phalloidin. A: Cell body at an end of a half-wrapped elliptical disk. (Scale bar: 10 μm.) B: Cell attached to flat side of an elliptical disk. (Scale bar: 5 μm.) C: Spherical particle attached to top of a cell. (Scale bar: 5 μm.) D–F: Actin reorganization–ring formation, polymerization at site of attachment, and start of internalization. (Scale bars in D-F: 10 μm). Reprinted with permission from [17]. Copyright (2006) National Academy of Sciences, USA. (**b**) Analysis of the wrapping fraction for phagocytosis for a spherical bead with $R = 2.3\,\mu\text{m}$. Initially, slow engulfment (light gray) is followed by a much quicker engulfment (dark gray). Insets show snapshots of the data that has been analyzed (blue: cell, red: bead, green: outline of pipette, and yellow: attached membrane). Reprinted with permission from [88], Copyright (2014), with permission from Elsevier. (**c**) Dynamical regulation of membrane tension during phagocytosis. After bead engagement (1), signaling is activated and actin polymerization pushes the membrane forward around the particle (2). Membrane tension increases because of protrusion, leading to membrane buffer (folds) depletion. High membrane tension leads to deactivation of signaling, actin reorganization, and activation of exocytosis (3). Increase of membrane area by actin-associated exocytosis (4) and complete engulfment (5). Reprinted with permission from [71]

the particle is completely engulfed via a zipper-like mechanism. Fast wrapping is also observed in the absence of receptors on half of the particle [47]. For elongated particles, such as prolate ellipsoidal particles, internalization is most efficient when the particles are wrapped tip-first; this is also predicted by calculations [88, 108]. These results suggest that phagocytic uptake is a combination of passive wrapping with a competition of adhesion and deformation energy and active, regulated cellular processes, such as cytoskeletal reorganization and formation of a phagocytic cup.

Despite longstanding efforts to unravel phagocytosis, the current understanding of the governing biophysical processes is limited. Therefore, efforts that interpret experimental data using theoretical models for active engulfment scenarios in biological cells are required to identify mechanisms. We discuss below some of these modeling approaches for active uptake.

In [108], a set of reaction–diffusion equations is used to model the dynamics of the signaling pathway. These equations are combined with an equation for the dynamics of the phagocytic cup and the deformation energy of the membrane. In agreement with experiments, this model predicts a mechanical bottleneck at half-wrapping as well as high uptake for spherical and prolate ellipsoidal particles and stalled phagocytosis for oblate ellipsoidal particles.

An alternative mechanism is described in [71] that suggests that the biphasic process for pseudopod formation during phagocytosis is regulated by plasma membrane tension. In the first phase of phagocytosis, a particle is wrapped until a buffer for membrane area that is stored in folds and ruffles is depleted after about half-wrapping. Hereafter, phagocytosis can only proceed if the tension of the plasma membrane is again lowered. This occurs during the second phase of phagocytosis by fusion of exocytic vesicles with the plasma membrane that enlarge its area and decrease its tension. Figure 12c illustrates this process.

A zipper mechanism for phagocytic uptake is proposed and investigated in [101]. Monte Carlo simulations for a fluctuating membrane are combined with adhesive particles of different shapes. The deformation energy is modeled using a triangulated membrane with the bending energy given by the Helfrich Hamiltonian. For the adhesive interaction, the vertices of the membrane close to the particle either gain a finite adhesion energy and attach reversibly or stick irreversibly. These two interactions model passive adhesion and an active zipper mechanism, respectively. The model suggests an increased importance of active wrapping with increasing particle size and also predicts the mechanical bottleneck where cups get stalled at or before half-wrapping. Furthermore, it reproduces the dependence of uptake on the orientation for prolate ellipsoidal particles, tip-first uptake is faster than side-first uptake.

Finite-element calculations for the membrane include the adhesive interaction between cell surface and target, mimic actin cytoskeletal polymerization at the leading edge, and invoke contractility at the cell–bead interface [56, 57]. Using this model, shapes for the phagocytic cups can be obtained that are similar to those observed experimentally during uptake.

A two-stage model assumes passive adhesion by receptor-mediated interaction that is limited by receptor diffusion in the first phase, and active mechanisms with directed motion of the receptors and signaling in the second phase [88]. This model is consistent with slow wrapping in the first phase and fast wrapping in the second phase, as observed in experiments. It also reproduces the observed quicker uptake when prolate ellipsoidal particles enter tip-first.

6 Conclusions and Outlook

With the advancement of technology, novel techniques to engineer nanoparticles of various shapes and sizes are now available. Such particles are obvious candidates for novel applications, therefore knowledge about their interaction in particular with plasma membranes as first step of their interaction with biological cells is required. A better understanding of the interaction of particles with biomembranes can facilitate development of drug and gene-delivery systems, advance the research on diseases by illuminating parasite and virus invasion, and may also help to develop strategies to engineer nanostructured surfaces for optimal cell adhesion to, e.g., biosensors. Soft particles, complex particle shapes, complex membrane compositions, more realistic calculations for dynamics of particle wrapping, and various active mechanisms, for example for phagocytic uptake, await further research both using theoretical and experimental techniques.

Acknowledgements Our research on the interaction of particles with biological membranes has been supported by the EU FP7 NMP collaborative project PreNanoTox (309666).

References

1. Abbena E, Salamon S, Gray A (2006) Modern differential geometry of curves and surfaces with Mathematica. Chapman and Hall/CRC, Boca Raton
2. Agudo-Canalejo J, Lipowsky R (2015) Critical particle sizes for the engulfment of nanoparticles by membranes and vesicles with bilayer asymmetry. ACS Nano 9(4):3704–3720
3. Atilgan E, Sun SX (2007) Shape transitions in lipid membranes and protein mediated vesicle fusion and fission. J Chem Phys 126(9):095102
4. Auth T, Gompper G (2009) Budding and vesiculation induced by conical membrane inclusions. Phys Rev E 80(3):031901
5. Auth T, Gov NS (2009) Diffusion in a fluid membrane with a flexible cortical cytoskeleton. Biophys J 96(3):818–830
6. Auth T, Safran SA, Gov NS (2007) Fluctuations of coupled fluid and solid membranes with application to red blood cells. Phys Rev E 76(5):051910
7. Bahrami AH, Lipowsky R, Weikl TR (2012) Tubulation and aggregation of spherical nanoparticles adsorbed on vesicles. Phys Rev Lett 109(18):188102
8. Bahrami AH et al (2014) Wrapping of nanoparticles by membranes. Adv Colloid Interf Sci 208:214–224
9. Bao G, Bao XR (2005) Shedding light on the dynamics of endocytosis and viral budding. Proc Natl Acad Sci USA 102(29):9997–9998
10. Barnoud J, Rossi G, Monticelli L (2014) Lipid membranes as solvents for carbon nanoparticles. Phys Rev Lett 112(6):068102
11. Barua S et al (2013) Particle shape enhances specificity of antibody-displaying nanoparticles. Proc Natl Acad Sci USA 110(9):3270–3275
12. Baumgart T, Hess ST, Webb WW (2003) Imaging coexisting fluid domains in biomembrane models coupling curvature and line tension. Nature 425(6960):821–824
13. Beningo KA, Wang Y-l (2002) Fc-receptor-mediated phagocytosis is regulated by mechanical properties of the target. J Cell Sci 115(4):849–856

14. Brakke KA (1992) The surface evolver. Exp Math 1(2):141–165
15. Brewster R, Pincus PA, Safran SA (2009) Hybrid lipids as a biological surface-active component. Biophys J 97(4):1087–1094
16. Canton I, Battaglia G (2012) Endocytosis at the nanoscale. Chem Soc Rev 41(7):2718–2739
17. Champion JA, Mitragotri S (2006) Role of target geometry in phagocytosis. Proc Natl Acad Sci USA 103(13):4930–4934
18. Champion JA, Katare YK, Mitragotri S (2007) Making polymeric micro-and nanoparticles of complex shapes. Proc Natl Acad Sci USA 104(29):11901–11904
19. Chaudhuri A, Battaglia G, Golestanian R (2011) The effect of interactions on the cellular uptake of nanoparticles. Phys Biol 8(4):046002
20. Chithrani BD, Chan WCW (2007) Elucidating the mechanism of cellular uptake and removal of protein-coated gold nanoparticles of different sizes and shapes. Nano Lett 7(6):1542–1550
21. Chithrani BD, Ghazani AA, Chan WCW (2006) Determining the size and shape dependence of gold nanoparticle uptake into mammalian cells. Nano Lett 6(4):662–668
22. Cho EC, Zhang Q, Xia Y (2011) The effect of sedimentation and diffusion on cellular uptake of gold nanoparticles. Nat Nanotech 6(6):385–391
23. Churchman AH et al (2013) Serum albumin enhances the membrane activity of ZnO nanoparticles. Chem Commun 49(39):4172–4174
24. Copolovici DM et al (2014) Cell-penetrating peptides: design, synthesis, and applications. ACS Nano 8(3):1972–1994
25. Cowman AF, Crabb BS (2006) Invasion of red blood cells by malaria parasites. Cell 124(4):755–766
26. Crick AJ et al (2014) Quantitation of malaria parasite-erythrocyte cell-cell interactions using optical tweezers. Biophys J 107(4):846–853
27. Dan N et al (1994) Membrane-induced interactions between inclusions. J Phys II (France) 4(10):1713–1725
28. Dasgupta S, Auth T, Gompper G (2013) Wrapping of ellipsoidal nano-particles by fluid membranes. Soft Matter 9(22):5473–5482
29. Dasgupta S, Auth T, Gompper G (2014) Shape and orientation matter for the cellular uptake of nonspherical particles. Nano Lett 14(2):687–693
30. Dasgupta S et al (2014) Membrane-wrapping contributions to malaria parasite invasion of the human erythrocyte. Biophys J 107(1):43–54
31. Dasgupta S, Auth T, Gompper G (2015) Wrapping of ellipsoidal nano-particles by fluid membranes. Soft Matter 11:7441–7444
32. Dasgupta S, Auth T, Gompper G (2017) Nano-and microparticles at fluid and biological interfaces. J Phys Condens Matter 29:373003
33. Decuzzi P, Ferrari M (2006) The adhesive strength of non-spherical particles mediated by specific interactions. Biomaterials 27(30):5307–5314
34. Decuzzi P, Ferrari M (2007) The role of specific and non-specific interactions in receptor-mediated endocytosis of nanoparticles. Biomaterials 28(18):2915–2922
35. Decuzzi P, Ferrari M (2008) The receptor-mediated endocytosis of nonspherical particles. Biophys J 94(10):3790–3797
36. Decuzzi P et al (2009) Intravascular delivery of particulate systems: does geometry really matter? Pharm Res 26(1):235–243
37. Deserno M (2004) Elastic deformation of a fluid membrane upon colloid binding. Phys Rev E 69(3):031903
38. Deserno M (2004) When do fluid membranes engulf sticky colloids? J Phys Condens Matter 16(22):S2061
39. Deserno M, Bickel T (2003) Wrapping of a spherical colloid by a fluid membrane. Europhys Lett 62(5):767
40. Deserno M, Gelbart WM (2002) Adhesion and wrapping in colloid-vesicle complexes. J Phys Chem B 106(21):5543–5552
41. Ding H-m, Tian W-de, Ma Y-q (2012) Designing nanoparticle translocation through membranes by computer simulations. ACS Nano 6(2):1230–1238

42. Ehrig J, Petrov EP, Schwille P (2011) Near-critical fluctuations and cytoskeleton-assisted phase separation lead to subdiffusion in cell membranes. Biophys J 100(1):80–89
43. Ewers H et al (2010) GM1 structure determines SV40-induced membrane invagination and infection. Nat Cell Biol 12(1):11–18
44. Fish et al MB (2015) Emergence and utility of nonspherical particles in biomedicine. Ind Eng Chem Res 54(16):4043–4059
45. Florez L et al (2012) How shape influences uptake: interactions of anisotropic polymer nanoparticles and human mesenchymal stem cells. Small 8(14):2222–2230
46. Fošnarič M et al (2009) Monte carlo simulations of complex formation between a mixed fluid vesicle and a charged colloid. J Chem Phys 131(10):105103
47. Gao Y, Yu Y (2013) How half-coated janus particles enter cells. J Am Chem Soc 135(51):19091–19094
48. Gao H, Shi W, Freund LB (2005) Mechanics of receptor-mediated endocytosis. Proc Natl Acad Sci USA 102(27):9469–9474
49. Ge P et al (2010) Cryo-em model of the bullet-shaped vesicular stomatitis virus. Science 327(5966):689–693
50. Gompper G, Kroll DM (2004) Triangulated surface models of fluctuating membranes. In: Nelson DR, Piran T, Weinberg S (eds) Statistical mechanics of membranes and surfaces. World Scientific, Singapore
51. Gózdz WT (2007) Deformations of lipid vesicles induced by attached spherical particles. Langmuir 23(10):5665–5669
52. Hamada T et al (2012) Size-dependent partitioning of nano/microparticles mediated by membrane lateral heterogeneity. J Am Chem Soc 134(34):13990–13996
53. Hansen JC et al (1997) Influence of network topology on the elasticity of the red blood cell membrane skeleton. Biophys J 72(5):2369
54. Hashemi SM, Sens P, Mohammad-Rafiee F (2014) Regulation of the membrane wrapping transition of a cylindrical target by cytoskeleton adhesion. J R Soc Interface 11(100):20140769
55. Helfrich W (1973) Elastic properties of lipid bilayers: theory and possible experiments. Z Naturforsch C 28(11–12):693–703
56. Herant M, Heinrich V, Dembo M (2006) Mechanics of neutrophil phagocytosis: experiments and quantitative models. J Cell Sci 119(9):1903–1913
57. Herant M et al (2011) Protrusive push versus enveloping embrace: computational model of phagocytosis predicts key regulatory role of cytoskeletal membrane anchors. PLoS Comput Biol 7(1):e1001068
58. Hoffmann I et al (2014) Softening of phospholipid membranes by the adhesion of silica nanoparticles–as seen by neutron spin-echo (NSE). Nanoscale 6(12):6945–6952
59. Huang C et al (2013) Role of nanoparticle geometry in endocytosis: laying down to stand up. Nano Lett 13(9):4546–4550
60. Hurley et al JH (2010) Membrane budding. Cell 143(6):875–887
61. Ivask A et al (2014) Size-dependent toxicity of silver nanoparticles to bacteria, yeast, algae, crustaceans and mammalian cells in vitro. PLOS One 9(7):e102108
62. Jaskiewicz K et al (2012) Incorporation of nanoparticles into polymersomes: size and concentration effects. ACS Nano 6(8):7254–7262
63. Jaskiewicz K et al (2012) Probing bioinspired transport of nanoparticles into polymersomes. Angew Chem 124(19):4691–4695
64. Killian JA (1998) Hydrophobic mismatch between proteins and lipids in membranes. Biochim Biophys Acta Rev Biomembr 1376(3):401–416
65. Koltover I, Raedler JO, Safinya CR (1999) Membrane mediated attraction and ordered aggregation of colloidal particles bound to giant phospholipid vesicles. Phys Rev Lett 82(9):1991
66. Le Bihan O et al (2009) Cryo-electron tomography of nanoparticle transmigration into liposome. J Struct Biol 168(3):419–425

67. Lesniak A et al (2012) Effects of the presence or absence of a protein corona on silica nanoparticle uptake and impact on cells. ACS Nano 6(7):5845–5857
68. Li S, Malmstadt N (2013) Deformation and poration of lipid bilayer membranes by cationic nanoparticles. Soft Matter 9(20):4969–4976
69. Lin J et al (2010) Penetration of lipid membranes by gold nanoparticles: insights into cellular uptake, cytotoxicity, and their relationship. ACS Nano 4(9):5421–5429
70. Lipowsky R (1992) Budding of membranes induced by intramembrane domains. J Phys II (France) 2(10):1825–1840
71. Masters TA et al (2013) Plasma membrane tension orchestrates membrane trafficking, cytoskeletal remodeling, and biochemical signaling during phagocytosis. Proc Natl Acad Sci USA 110(29):11875–11880
72. Michel R et al (2014) Internalization of silica nanoparticles into fluid liposomes: formation of interesting hybrid colloids. Angew Chem Int Ed 53(46):12441–12445
73. Mihut AM et al (2013) Tunable adsorption of soft colloids on model biomembranes. ACS Nano 7(12):10752–10763
74. Möller J et al (2012) The race to the pole: how high-aspect ratio shape and heterogeneous environments limit phagocytosis of filamentous escherichia coli bacteria by macrophages. Nano Lett 12(6):2901–2905
75. Monopoli MP et al (2012) Biomolecular coronas provide the biological identity of nanosized materials. Nat Nanotechnol 7(12):779–786
76. Monticelli L et al (2009) Effects of carbon nanoparticles on lipid membranes: a molecular simulation perspective. Soft Matter 5(22):4433–4445
77. Nicolson GL (2014) The fluid—mosaic model of membrane structure: still relevant to understanding the structure, function and dynamics of biological membranes after more than 40 years. Biochim Biophys Acta Rev Biomembr 1838(6):1451–1466
78. Noda T et al (2006) Assembly and budding of ebolavirus. PLoS Pathog 2(9):e99–e99
79. Nowak SA, Chou T (2008) Membrane lipid segregation in endocytosis. Phys Rev E 78(2):021908
80. Nowak SA, Chou T (2009) Mechanisms of receptor/coreceptor-mediated entry of enveloped viruses. Biophys J 96(7):2624–2636
81. Osaki F et al (2004) A quantum dot conjugated sugar ball and its cellular uptake. on the size effects of endocytosis in the subviral region. J Am Chem Soc 126(21):6520–6521
82. Park J-G, Forster JD, Dufresne ER (2010) High-yield synthesis of monodisperse dumbbell-shaped polymer nanoparticles. J Am Chem Soc 132(17):5960–5961
83. Pletikapić G et al (2012) Atomic force microscopy characterization of silver nanoparticles interactions with marine diatom cells and extracellular polymeric substance. J Mol Recognit 25(5):309–317
84. Pogodin S, Baulin VA (2010) Can a carbon nanotube pierce through a phospholipid bilayer? ACS Nano 4(9):5293–5300
85. Raatz M, Lipowsky R, Weikl TR (2014) Cooperative wrapping of nanoparticles by membrane tubes. Soft Matter 10(20):3570–3577
86. Reynwar BJ, Deserno M (2011) Membrane-mediated interactions between circular particles in the strongly curved regime. Soft Matter 7(18):8567–8575
87. Reynwar BJ et al (2007) Aggregation and vesiculation of membrane proteins by curvature-mediated interactions. Nature 447(7143):461–464
88. Richards DM, Endres RG (2014) The mechanism of phagocytosis: two stages of engulfment. Biophys J 107(7):1542–1553
89. Roiter Y et al (2008) Interaction of nanoparticles with lipid membrane. Nano Lett 8(3):941–944
90. Rossi G, Monticelli L (2014) Modeling the effect of nano-sized polymer particles on the properties of lipid membranes. J Phys Condens Matter 26(50):503101
91. Sackmann E (1995) Biological membranes architecture and function. In: Lipowsky R, Sackmann E (eds) Structure and dynamics of membranes. Elsevier, Amsterdam

92. Šarić A, Cacciuto A (2011) Soft elastic surfaces as a platform for particle self-assembly. Soft Matter 7(18):8324–8329
93. Šarić A, Cacciuto A (2012) Fluid membranes can drive linear aggregation of adsorbed spherical nanoparticles. Phys Rev Lett 108(11):118101
94. Šarić A, Cacciuto A (2012) Mechanism of membrane tube formation induced by adhesive nanocomponents. Phys Rev Lett 109(18):188101
95. Šarić A, Cacciuto A (2013) Self-assembly of nanoparticles adsorbed on fluid and elastic membranes. Soft Matter 9(29):6677–6695
96. Schäfer LV et al (2011) Lipid packing drives the segregation of transmembrane helices into disordered lipid domains in model membranes. Proc Natl Acad Sci USA 108(4):1343–1348
97. Smith KA, Jasnow D, Balazs AC (2007) Designing synthetic vesicles that engulf nanoscopic particles. J Chem Phys 127(8):084703
98. Sondi I, Salopek-Sondi B (2004) Silver nanoparticles as antimicrobial agent: a case study on e. coli as a model for gram-negative bacteria. J Colloid Int Sci 275(1):177–182
99. Taturet S et al (2013) Effect of functionalized gold nanoparticles on floating lipid bilayers. Langmuir 29(22):6606–6614
100. Tian F, Zhang X, Dong W (2014) How hydrophobic nanoparticles aggregate in the interior of membranes: a computer simulation. Phys Rev E 90(5):052701
101. Tollis S et al (2010) The zipper mechanism in phagocytosis: energetic requirements and variability in phagocytic cup shape. BMC Syst Biol 4(1):149
102. Tzlil S et al (2004) A statistical-thermodynamic model of viral budding. Biophys J 86(4):2037–2048
103. Upadhyaya A, Sheetz MP (2004) Tension in tubulovesicular networks of golgi and endoplasmic reticulum membranes. Biophys J 86(5):2923–2928
104. Vácha R, Martinez-Veracoechea FJ, Frenkel D (2011) Receptor-mediated endocytosis of nanoparticles of various shapes. Nano Lett 11(12):5391–5395
105. Van Lehn RC, Alexander-Katz A (2014) Fusion of ligand-coated nanoparticles with lipid bilayers: effect of ligand flexibility. J Phys Chem A 118(31):5848–5856
106. Van Lehn RC, Alexander-Katz A (2014) Membrane-embedded nanoparticles induce lipid rearrangements similar to those exhibited by biological membrane proteins. J Phys Chem B 118(44):12586–12598
107. Van Lehn RC et al (2014) Lipid tail protrusions mediate the insertion of nanoparticles into model cell membranes. Nat Commun 5:Article No 4482
108. van Zon JS et al (2009) A mechanical bottleneck explains the variation in cup growth during fcγr phagocytosis. Mol Syst Biol 5(1):298
109. Vandoolaeghe P et al (2008) Adsorption of cubic liquid crystalline nanoparticles on model membranes. Soft Matter 4(11):2267–2277
110. Vasir JK, Labhasetwar V (2008) Quantification of the force of nanoparticle-cell membrane interactions and its influence on intracellular trafficking of nanoparticles. Biomaterials 29(31):4244–4252
111. Verma A et al (2008) Surface-structure-regulated cell-membrane penetration by monolayer-protected nanoparticles. Nat Mater 7(7):588–595
112. Wang T et al (2012) Cellular uptake of nanoparticles by membrane penetration: a study combining confocal microscopy with FTIR spectroelectrochemistry. ACS Nano 6(2):1251–1259
113. Welsch S et al (2010) Electron tomography reveals the steps in filovirus budding. PLoS Pathog 6(4):e1000875
114. Werner M, Sommer J-U, Baulin VA (2012) Homo-polymers with balanced hydrophobicity translocate through lipid bilayers and enhance local solvent permeability. Soft Matter 8(46):11714–11722
115. Wu H-J et al (2012) Membrane-protein binding measured with solution-phase plasmonic nanocube sensors. Nat Methods 9:1189–1191
116. Yang K, Ma Y-Q (2010) Computer simulation of the translocation of nanoparticles with different shapes across a lipid bilayer. Nat Nanotechnol 5(8):579–583

117. Yi X, Gao H (2015) Cell membrane wrapping of a spherical thin elastic shell. Soft Matter 11(6):1107–1115
118. Yi X, Shi X, Gao H (2011) A universal law for cell uptake of one-dimensional nanomaterials. Nano Lett 107(9):098101
119. Yi X, Shi X, Gao H (2014) Cellular uptake of elastic nanoparticles. Phys Rev Lett 14(2):1049–1055
120. Yuan H et al (2010) Variable nanoparticle-cell adhesion strength regulates cellular uptake. Phys Rev Lett 105(13):138101
121. Yue T, Zhang X (2013) Molecular modeling of the pathways of vesicle–membrane interaction. Soft Matter 9(2):559–569
122. Zemel A, Ben-Shaul A, May S (2005) Perturbation of a lipid membrane by amphipathic peptides and its role in pore formation. Eur Biophys J 34(3):230–242
123. Zhang S et al (2009) Size-dependent endocytosis of nanoparticles. Adv Mater 21(4):419–424
124. Zhang Y et al (2012) Permission to enter cell by shape: nanodisk vs nanosphere. ACS Appl Mater Interfaces 4(8):4099–4105